International Journal of Minerals, Metallurgy and Materials
Volume 21, Number 3, March 2014, Page 225
DOI: 10.1007/s12613-014-0889-6

Metalizing reduction and magnetic separation of vanadium titano-magnetite based on hot briquetting

Shuang-yin Chen and Man-sheng Chu

School of Materials and Metallurgy, Northeastern University, Shenyang 110819, China
(Received: 12 September 2013; revised: 19 November 2013; accepted: 20 November 2013)

Abstract: To achieve high efficiency utilization of Panzhihua vanadium titano-magnetite, a new process of metalizing reduction and magnetic separation based on hot briquetting is proposed, and factors that affect the cold strength of the hot-briquetting products and the efficiency of reduction and magnetic separation are successively investigated through laboratory experiments. The relevant mechanisms are elucidated on the basis of microstructural observations. Experimental results show that the optimal process parameters for hot briquetting include a hot briquetting temperature of 475°C, a carbon ratio of 1.2, ore and coal particle sizes of less than 74 μm. Additionally, with respect to metalizing reduction and magnetic separation, the rational parameters include a magnetic field intensity of 50 mT, a reduction temperature of 1350°C, a reduction time of 60 min, and a carbon ratio of 1.2. Under these above conditions, the crushing strength of the hot-briquetting agglomerates is 1480 N, and the recovery ratios of iron, vanadium, and titanium are as high as 91.19%, 61.82%, and 85.31%, respectively. The new process of metalizing reduction and magnetic separation based on hot briquetting demonstrates the evident technological advantages of high efficiency separation of iron from other valuable elements in the vanadium titano-magnetite.

Keywords: magnetite; hot briquetting; ore reduction; magnetic separation

1. Introduction

Vanadium titano-magnetite (VTM) owes its extremely high comprehensive utilization value due to abundantly associating valuable elements (i.e., iron, vanadium, and titanium). The reserve of VTM resources is greater than 10 billion tons in the Panzhihua and Xichang regions of China, where the amounts of titanium and vanadium account for 93% and 63%, respectively, of the national total reserves [1–2].

Because of its drawbacks, which include its poor grade, fine mineral crystal size, complicated phase structure, and numerous mineral components [3], VTM is classified as a typical polymetallic paragenic resource that is difficult to treat and utilize [4]. Currently, the mainstream route of the comprehensive utilization of VTM is blast furnace (BF) ironmaking → basic oxygen furnace (BOF) vanadium extraction → semisteel smelting. However, the critical shortcoming of the BF-BOF process is its lower utilization of resources. For example, the recovery ratios of iron, vanadium, and titanium are just 70%, 47%, and 25%, respectively. In addition, 70 million tons of titanium-containing BF slag is discarded and deposited onto the riversides of the Jinsha River, resulting in severe environmental pollution and a waste of resources [5–6]. Thus, a great number of new comprehensive utilization processes have been proposed and studied, including chemical extraction, direct reduction (e.g., via a fluidized bed, rotary kiln, rotary hearth furnace), and EAF smelting [7–12]. Although some of these processes have been extensively studied and some have even been verified through semi-industrialization tests, none have been successfully put into industrial use. The key problem is that the selective separation and comprehensive utilization of valuable elements have not been achieved in an economical and efficient way [7–12]. Therefore, high efficiency and clean utilization of VTM has become the subject of important national projects and is important to the sustainable development of the metallurgy industry [13–14].

On the basis of the previously discussed background, a new comprehensive utilization process for VTM (i.e.,

Corresponding author: Man-sheng Chu E-mail: chums@smm.neu.edu.cn

metalizing reduction and magnetic separation based on hot briquetting) is put forth in this study. Fig. 1 shows a flowchart of the new process, in which hot briquetting agglomerates of the VTM with sufficiently high strength are first produced and subjected to carbothermal reduction under appropriate conditions. The iron components in the reduction products are subsequently separated from the vanadium-titanium-bearing slag using a magnetic dressing machine. Finally, the slag can be further treated via hydrometallurgy.

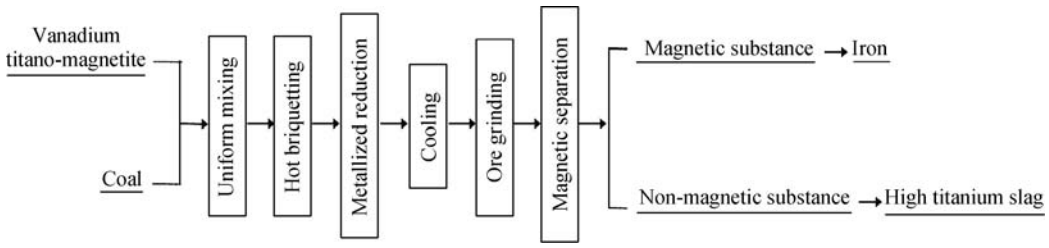

Fig. 1. Flowchart of the new process proposed in this study.

The previous research based on fine powders of VTM and coal has revealed that the method of metalizing reduction and magnetic separation is effective in achieving an efficient separation of iron from other elements in VTM [15]; however, this method is not feasible on an industrial scale because of low ore-treating capacity and the difficulty involved in selecting appropriate reactor equipment. Given the high strength and fast reduction speed of hot-briquetting agglomerates [16], a process based on hot briquetting would successfully resolve the shortcomings of the process based on fine powders. Therefore, in this paper, we focus on our investigation of the effects of major process parameters on hot briquetting, metalizing reduction, and magnetic separation, thereby elucidating the relevant mechanism of separation of valuable elements. We also explore the feasibility of this innovative process of metalizing reduction and magnetic separation based on hot briquetting, which may establish a solid foundation for the high efficiency and comprehensive utilization of VTM.

2. Experimental

2.1. Raw materials

The chemical compositions of the VTM ore and coal used in this study are listed in Table 1. The VTM from Panzhihua region contains 53.91wt% Fe, 13.03wt% TiO_2, and 0.52wt% V_2O_5. The coal used for hot briquetting is a kind of bitumite with a certain thermal plasticity and a fixed carbon content of 50.94wt%.

Table 1. Chemical composition of VTM and coal used in this study wt%

VTM								Coal				
TFe	FeO	V_2O_5	TiO_2	CaO	SiO_2	MgO	Al_2O_3	A_{ad}	V_{daf}	M_{ad}	S_{td}	FC
53.91	31.13	0.52	13.03	0.68	3.20	2.71	3.82	14.00	33.70	1.36	0.02	50.94

Note: A_{ad} — ash content on air dry basis; V_{daf} — volatile matter content on dry ash free basis; M_{ad} — moisture on air dry basis; S_{td} — total sulfur content on dry basis; FC — fixed carbon content.

The X-ray diffraction pattern of the VTM is shown in Fig. 2. The VTM mainly consists of magnetite (Fe_3O_4), titanomagnetite ($Fe_3Ti_{3-x}O_4$), ilmenite ($FeTiO_3$), and vanadium spinel ($FeO{\cdot}V_2O_3$).

2.2. Experimental procedure

Fig. 3 shows a schematic diagram of the experimental procedure and equipment.

The first step is the preparation of hot briquetting agglomerates and testing of their cold strength according to national standards (GB/T14201–93) [17–18]. During the tests, the process parameters of hot briquetting, specifically,

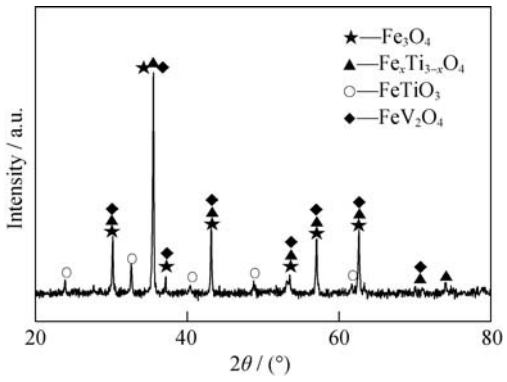

Fig. 2. XRD pattern of the VTM used in this study.

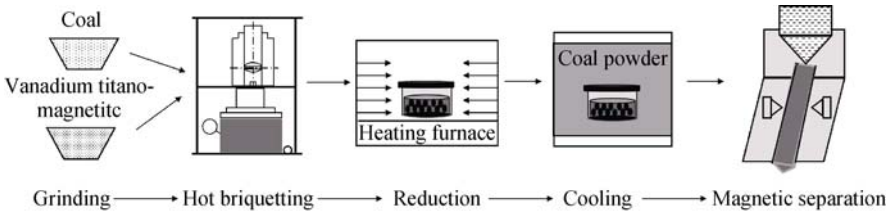

Fig. 3. Schematic diagram of the experiment procedure and equipment.

the carbon ratio, the hot briquetting temperature, and the VTM and coal particle sizes, are changed within preset ranges, and the optimal parameters are determined on the basis of orthogonal experiment method. The second step involves carbothermal reduction experiments of hot briquetting agglomerates, where the agglomerates are added into a graphite crucible, placed in a high-temperature furnace, and reduced at the preset temperature for the preset time. The third step involves magnetic dressing experiments of cooled reduction products. During the study, the effects of major process parameters, including the magnetic field intensity, the reduction time, the reduction temperature, and the carbon ratio, on the dressing efficiency were successively analyzed. We conducted elemental analysis and XRD and SEM measurement for the magnetic substance and nonmagnetic substance obtained after dressing to calculate the reduction and dressing process index and to elucidate the relevant mechanisms.

3. Results and discussion

3.1. Preparation and strength of hot-briquetting agglomerates

During preliminary experiments of hot briquetting, the hydraulic cylinder pressure was varied from 30 MPa to 40 MPa to 50 MPa. After taking the agglomerate strength and process flexibility into account, we determined that the pressure of 40 MPa was best suited for the subsequent experiments. Notably, we conducted orthogonal tests to explore the effects of several key factors on the cold strength of the hot-briquetting products. The scheme of the orthogonal experiments is detailed in Table 2. Four key process factors and four varying levels were used, including a carbon ratio of 0.8–1.4, a hot-briquetting temperature of 400–475°C, a VTM particle size range of −150 μm (less than 150 μm, −100 mesh) to −74 μm (less than 74 μm, −200 mesh), and a coal particle size range from −150 μm to −74 μm. The results of each orthogonal experiment are also listed in Table 2.

Table 3 gives the results of the orthogonal range analysis for the data listed in Table 2. These results quantitatively indicate the significance of each key process factor on the cold strength of hot-briquetting agglomerates and the optimal value of each factor. According to Table 3, the hot-briquetting temperature most strongly affects the cold strength of the hot-briquetting products, followed successively by the carbon ratio, the coal particle size, and the VTM particle size. The optimal hot-briquetting process parameters include a hot-briquetting temperature of 475°C, a carbon ratio of 1.4, and VTM and coal particles sizes of less than 74 μm.

Table 2. Scheme and results of orthogonal experiments

No.	*A*	*B* / °C	*C* / μm	*D* / μm	Cold strength / N	No.	*A*	*B* / °C	*C* / μm	*D* / μm	Cold strength / N
1	0.8	400	−106	−74	643.3	9	1.2	400	−74	−150	818.9
2	0.8	425	−150	−80	745.5	10	1.2	425	−106	−106	821.0
3	0.8	450	−80	−150	1173.3	11	1.2	450	−150	−74	1324.4
4	0.8	475	−74	−106	1092.9	12	1.2	475	−106	−80	1463.4
5	1.0	400	−80	−80	633.0	13	1.4	400	−150	−150	971.8
6	1.0	425	−74	−74	1017.7	14	1.4	425	−106	−150	950.4
7	1.0	450	−106	−106	816.3	15	1.4	450	−74	−80	1529.4
8	1.0	475	−150	−150	993.8	16	1.4	475	−80	−74	1387.9

Note: *A* — Carbon ratio; *B* — Hot-briquetting temperature; *C* — VTM size; *D* — Coal size.

In addition, because an excessive carbon ratio will diminish the strength of hot-briquetting agglomerates, the carbon ratio should be maintained at approximately 1.2 [18]. Thus, the rational hot-briquetting process parameters obtained in this study include a hot-briquetting temperature of 475°C, a carbon ratio of 1.2, and VTM and coal particle

sizes of less than 74 μm. Under these conditions, the cold strength of the hot-briquetting agglomerates was 1480 N, which is evidently higher than that of common cold-bonded agglomerates and should satisfy the technological requirements of reduction equipment, such as a coal-based shaft furnace, for future industrial applications.

Table 3. Range analysis of the orthogonal experimental results

Factor	*A*	*B*	*C*	*D*
k_1	913.8	766.8	1008.9	984.1
k_2	865.2	883.7	968.4	925.5
k_3	1106.9	1210.9	1003.8	1092.8
k_4	1209.9	1234.5	1114.7	1093.3
R	344.7	467.7	146.3	167.8
Significance	$R_B > R_A > R_D > R_C$			
Optimum	A_4	B_4	C_4	D_4

Note: *A* — Carbon ratio; *B* — Hot-briquetting temperature; *C* — VTM size; *D* — Coal size.

3.2. Effects of magnetic field intensity

To determine the optimum magnetic field intensity, we separated the reduction product using a DTCXG–ZN50 magnetic tube under a magnetic field intensity between 25 and 125 mT while keeping the other process parameters constant (i.e., a reduction temperature of 1350°C, a reduction time of 60 min, and a carbon ratio of 1.2).

The chemical compositions and metallization rate of the reduction product under the previously described conditions are listed in Table 4, and the effects of the magnetic field intensity on the separation of the valuable elements are described in Fig. 4. After magnetic separation, iron enters a magnetic phase, whereas vanadium and titanium form a nonmagnetic substance. As shown in Fig. 4, the vanadium content ($w(V_2O_5)$), the recovery ratio of vanadium ($\eta(V_2O_5)$), the titanium content ($w(TiO_2)$), and the recovery ratio of titanium ($\eta(TiO_2)$) in the nonmagnetic substance evidently increase as the magnetic field intensity is increased from 25 mT to 50 mT but decrease when the magnetic field intensity is greater than 50 mT. In addition, the total iron content (TFe) in the magnetic substance also exhibits a similar tendency. Thus, the optimal magnetic field intensity was determined to be approximately 50 mT for the subsequent experiments.

Table 4. Chemical composition and metallization rate of the reduction product wt%

TFe	MFe	V_2O_5	TiO_2	Metallization rate
65.22	61.06	0.676	13.67	93.62

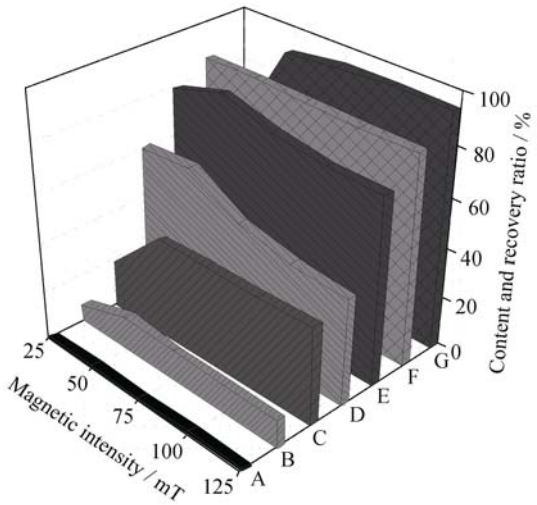

A: $w(V_2O_5)$; B: $10 \times w(V_2O_5)$; C: $\eta(V_2O_5)$; D: $w(TiO_2)$; E: $\eta(TiO_2)$; F: TFe; G: η(Fe)

Fig. 4. Effects of magnetic field intensity on the separation of valuable elements.

The relevant mechanisms were analyzed on the basis of SEM and EDS measurements of the previously described reduction product, as shown in Fig. 5. Figs. 5(a) and 5(b) show that the dispersed iron particles (white phase "A") are formed and integrate with each other due to metallization reduction and carburization. Figs. 5(a) and 5(c) show that nonmagnetic high-titanium slag (gray phase "B") moved to the surface of the magnetic iron phase and attached to tiny iron particles, which deleteriously affected the magnetic separation of the iron phase from the other phases. When the magnetic field intensity was increased beyond a certain value, more high-titanium slag was entrained and wrapped into the magnetic substance because of the excessive magnetic force, which led to the diminished recovery of vanadium and titanium.

3.3. Effects of reduction temperature

To optimize the reduction temperature, we performed a series of reduction and magnetic dressing tests at various reduction temperatures, including 1275°C, 1300°C, 1325°C, and 1350°C. The other parameters were kept constant as follows: a reduction time of 60 min, a carbon ratio of 1.2, and a magnetic field intensity of 50 mT.

Under these conditions, the effects of the reduction temperature on the metallization rate of the reduction product are shown in Fig. 6. The metallization rate of the reduction products increased gradually with increasing reduction temperature. When the reduction temperature was 1350°C, the metallization rate reached 93.62wt%.

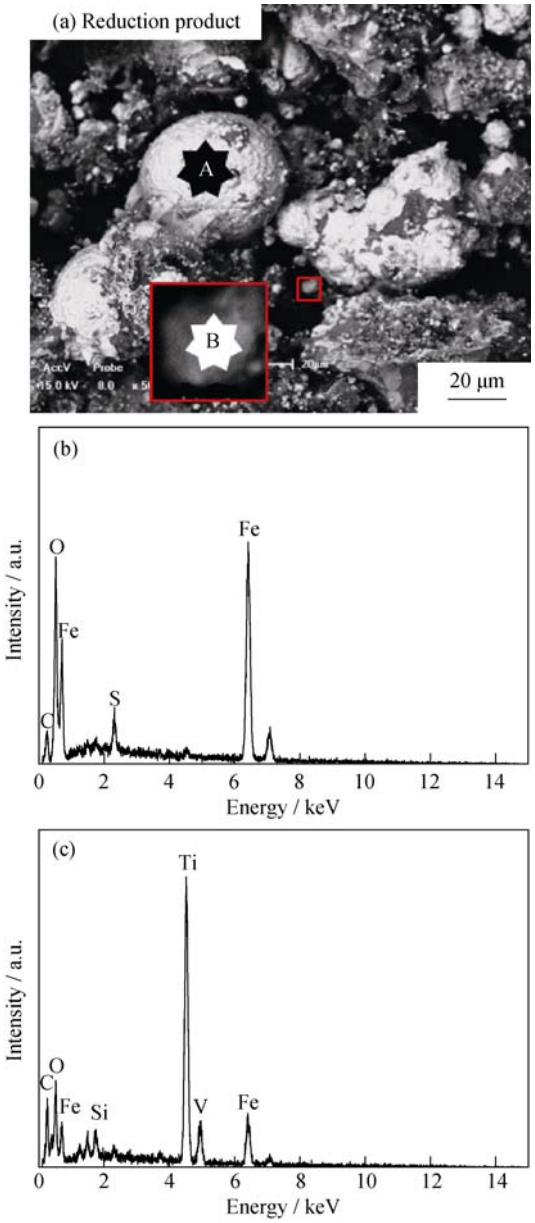

Fig. 5. SEM image and EDS spectra of the reduction products: (a) SEM; (b) EDS of A point in (a); (c) EDS of B point in (a).

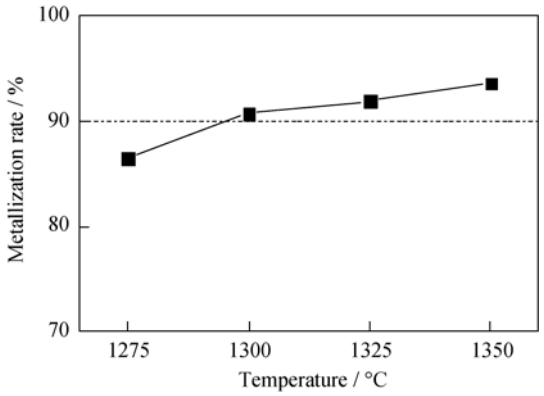

Fig. 6. Effects of reduction temperature on the metallization rate of the reduction products.

The effects of the reduction temperature on the separation of the valuable elements are described in Fig. 7. The total iron content and recovery ratio of iron in the magnetic phase significantly increased after the magnetic dressing process. In addition, the titanium content, the recovery ratio of titanium, the vanadium content, and the recovery ratio of vanadium in the nonmagnetic substance also improved with increasing temperature. Corresponding to reduction temperatures of 1275, 1300, 1325, and 1350°C, the η(Fe) was 89.20%, 89.25%, 90.17%, and 91.19%, the $\eta(V_2O_5)$ was 36.25%, 50.59%, 56.41%, and 61.41%, and the $\eta(TiO_2)$ was 48.99%, 75.43%, 83.95%, and 84.74%, respectively. Synthetically, given the heating capacity of industrial reduction equipment and the high recovery of iron, vanadium, and titanium, we determined that the reduction temperature should be no lower than 1350°C in the subsequent experiments.

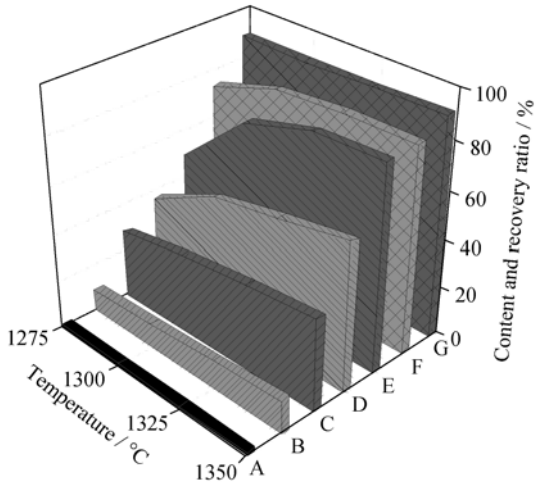

A: $w(V_2O_5)$; B: $10 \times w(V_2O_5)$; C: $\eta(V_2O_5)$; D: $w(TiO_2)$; E: $\eta(TiO_2)$; F: TFe; G: η(Fe)

Fig. 7. Effects of the reduction temperature on the separation of the valuable elements.

SEM photos of the four kinds of reduction products are shown in Fig. 8. With an increase in the reduction temperature, the thermodynamic and kinetic conditions of the reduction of the iron-bearing phase should be remarkably improved. The nucleation, aggregation, and growth of the reduced iron particles are further facilitated and much larger iron bead is formed at 1350°C. Thus, the effect of separating the iron phases from the other phases will be much more obvious at higher reduction temperatures.

3.4. Effects of reduction time

According to the method that is similar to the experiments related to the reduction temperature, a series of reduc-

tion and magnetic dressing tests were performed using various reduction times, including 10 min, 20 min, 30 min, 40 min, 50 min, and 60 min, while the other parameters were kept constant as follows: a reduction temperature of 1350°C, a carbon ratio of 1.2, and a magnetic field intensity of 50 mT.

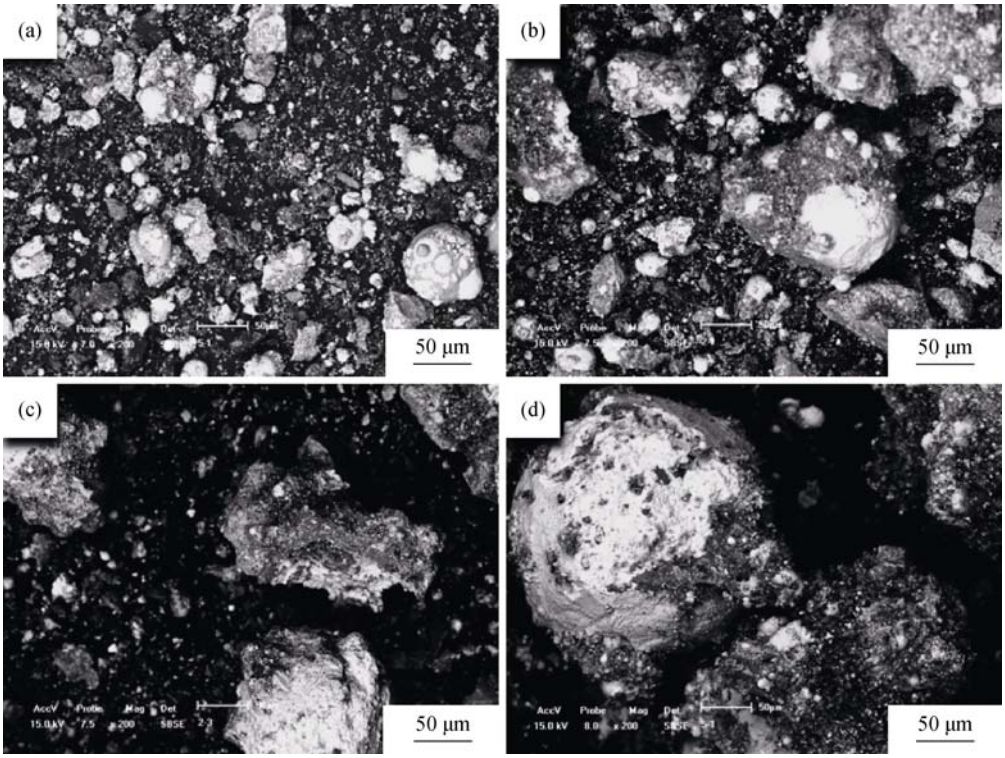

Fig. 8. SEM images of reduction products obtained at different reduction temperatures: (a) 1275°C; (b) 1300°C; (c) 1325°C; (d) 1350°C.

The effects of reduction time on the metallization rate of the reduction products are shown in Fig 9. Within the experimental range, the metallization rate of the reduction products showed an increase tendency with increasing reduction time and reached a rate of 92.33% at a reduction time of 60 min.

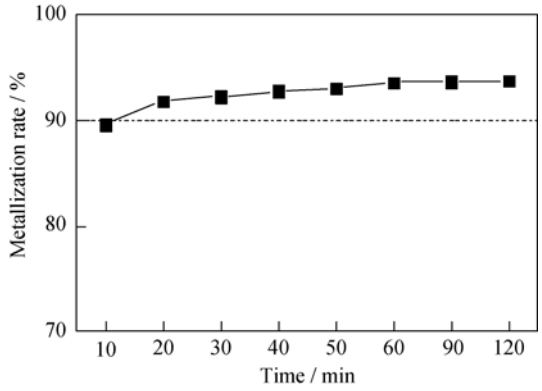

Fig. 9. Effect of reduction time on the metallization rate of the reduction products.

The effects of reduction time on the separation of the valuable elements are described in Fig. 10. The total iron content of iron phase in the magnetic substance significantly increased with increasing reduction time, and the iron recovery ratios were all greater than 90%. In general, the titanium content, the recovery ratio of titanium, the vanadium content, and the recovery ratio of vanadium in the nonmagnetic substance all improved with increasing reduction time. Corresponding to reduction times of 10 min, 40 min, 50 min, and 60 min, the recovery of iron was 90.09%, 94.53%, 92.54%, and 91.19%, the recovery of vanadium was 33.50%, 35.98%, 44.92%, and 61.82%, and the recovery of titanium was 51.09%, 76.73%, 75.47%, and 85.31%, respectively. Given the industrial production efficiency and the high recovery of iron, vanadium, and titanium, we determined that the rational reduction time should be no shorter than 60 min for the subsequent experiments. The relevant mechanisms are similar to those responsible for the effects of the reduction temperature. When the reduction time is prolonged, nucleation, aggregation, and growth of reduced iron particles are fully developed, which contributes to the formation of a larger iron bead and results in improved separation of iron phase from the other phases.

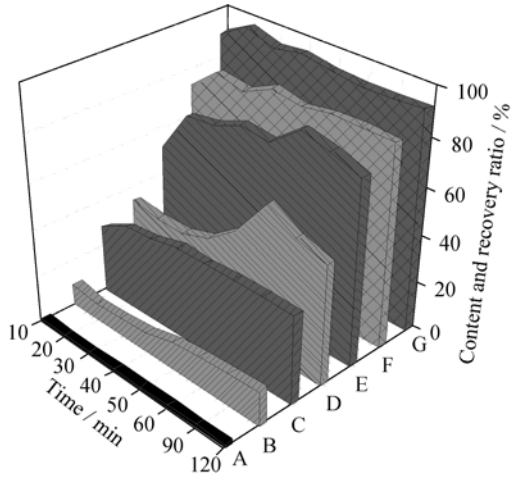

A: $w(V_2O_5)$; B: 10 × $w(V_2O_5)$; C: $\eta(V_2O_5)$; D: $w(TiO_2)$; E: $\eta(TiO_2)$; F: TFe; G: η(Fe)

Fig. 10. Effects of reduction time on the separation of the valuable elements.

3.5. Effects of carbon ratio

The last set of experiments was conducted to investigate the effects of the carbon ratio. During the study, the carbon ratio of the hot-briquetting agglomerates were varied from 0.8 to 1.0, 1.2, and 1.4, in conjunction with a reduction temperature of 1350°C, a reduction time 60 min, and magnetic field intensity 50 mT.

The effects of the carbon ratio on the metallization rate of the reduction products are shown in Fig. 11. The carbon ratio had no remarkable effects on the metallization rate, which fluctuated at approximately 94.00%.

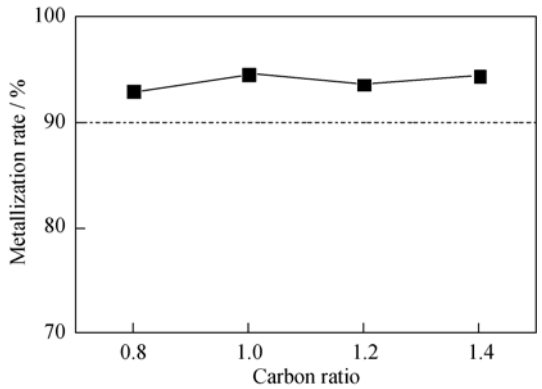

Fig. 11. Effect of carbon ratio on the metallization rate of the reduction products.

The effects of the carbon ratio on the separation of the valuable elements are shown in Fig. 12. When the carbon ratio was increased from 0.8 to 1.2, the total iron content in the magnetic substance and the vanadium content, the recovery ratio of vanadium, the titanium content, and the recovery ratio of titanium in the nonmagnetic substance increased from 84.26% to 85.90%, from 1.04% to 1.40%, from 38.75% to 61.82%, from 38.11% to 39.12%, and from 73.90% to 85.31%, respectively. When the carbon ratio was further increased to 1.4, the values of indexes all tended to decrease. As a result, the optimal carbon ratio for the VTM hot-briquetting agglomerates should be maintained at approximately 1.2.

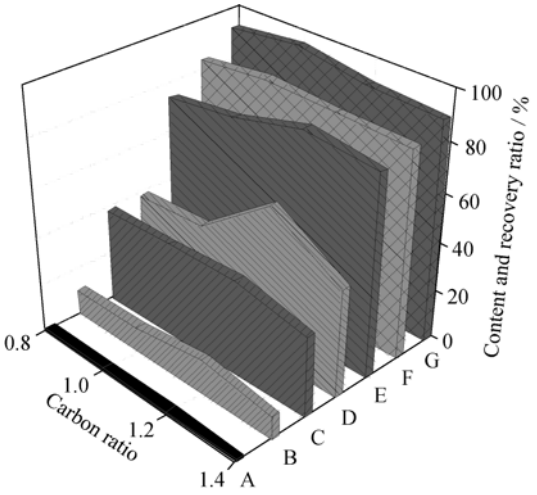

A: $w(V_2O_5)$; B: 10 × $w(V_2O_5)$; C: $\eta(V_2O_5)$; D: $w(TiO_2)$; E: $\eta(TiO_2)$; F: TFe; G: η(Fe)

Fig. 12. Effects of carbon ratio on the separation of the valuable elements.

Fig. 13 shows SEM photos of the reduction products obtained with different carbon ratios, where the white particles represent for iron-containing phases. The results show that, when the carbon ratio was increased from 0.8 to 1.2, iron particles formed, aggregated, and grew much larger due to the supply of sufficient carbon for both direct reduction and carburization, as shown in Figs. 13(a)–13(c). However, when the carbon ratio was further increased to 1.4, the carbon supply became excessive and much more graphitized carbon was formed; this graphitized carbon prevented the aggregation of reduced iron particles and resulted in the formation of only relatively smaller iron particles, which ultimately led to poor separation of Fe-containing phases from the other phases, as shown in Fig. 13(d).

4. Conclusions

(1) Via the orthogonal analysis of hot-briquetting experiments, the rational process parameters were obtained as follows: a hot briquetting temperature of 475°C, a carbon ratio of 1.2, VTM and coal particle sizes less than 74 μm, and a cold strength of the hot-briquetting products as high as 1480 N.

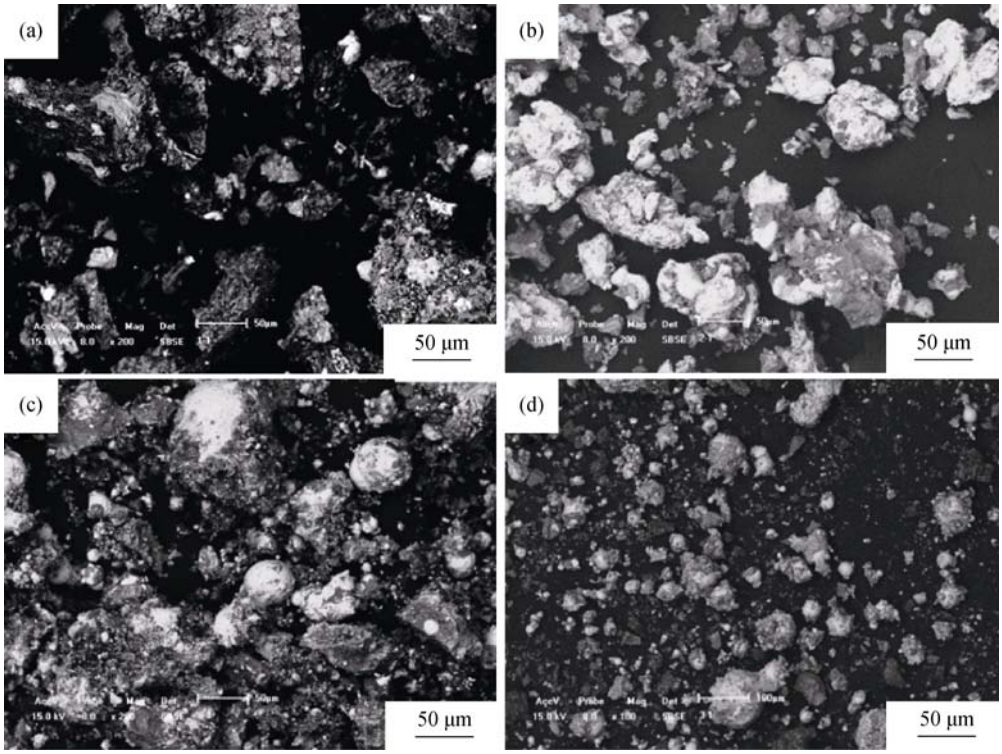

Fig. 13. SEM images of the reduction products with different carbon ratios: (a) 0.8; (b) 1.0; (c) 1.2; (d) 1.4.

(2) The rational process conditions for the metalizing reduction and magnetic separation include a carbon ratio of 1.2, a reduction temperature of 1350°C, a reduction time of 60 min, and a magnetic field intensity of 50 mT.

(3) The new process of metalizing reduction, and magnetic separation of vanadium titano-magnetite based on hot briquetting should enable the high efficiency separation of iron from vanadium and titanium. Under the previously described rational process conditions, the recovery ratio of iron in the magnetic substance is 91.19%, and the recovery ratios of vanadium and titanium in the nonmagnetic substance are 61.82% and 85.31%, respectively.

Acknowledgements

This study was financially supported by the National High-Tech Research and Development Program of China (No. 2012AA062302), the Major Program of the National Natural Science Foundation of China (No. 51090384), and the Fundamental Research Funds of the Central Universities of China (No. N110202001).

References

[1] J. Barksdale, *Titanium: Its Occurrence*, *Chemistry*, *and Technology*, 2nd edition, The Roland Press Company, New York, 1966, p. 1.

[2] D.S. Chen, B. Song, L.N. Wang, T. Qi, Y. Wang, and W.J. Wang, Solid state reduction of Panzhihua titanomagnetite concentrates with pulverized coal, *Miner. Eng.*, 24(2011), No. 8, p. 864.

[3] T. Hu, X.W. Lv, C.G. Bai, Z.G. Lun, and G.B. Qiu, Reduction behavior of Panzhihua titanomagnetite concentrates with coal, *Metall. Mater. Trans. B*, 44(2013), No. 2, p. 252.

[4] X.G. Si, X.G. Lu, C.W. Li, C.H. Li, and W.Z. Ding, Phase transformation and reduction kinetics during the hydrogen reduction of ilmenite concentrate, *Int. J. Miner. Metall. Mater.*, 19(2012), No. 5, p. 384.

[5] R.S. Diao, New understanding about special problems of smelting vanadium-bearing titanomagnetite with BF, *Iron Steel*, 34(1999), No. 6, p. 12.

[6] J.Y. Ma, X.W. Sun, and S.X. Sheng, Intensified smelting of vanadium and titanium magnetite in blast furnace, *Iron Steel*, 35(2000), No. 1, p. 4.

[7] R. Huang, X.W. Lv, C.G. Bai, Q.Y. Deng, and S.W. Ma, Solid state and smelting reduction of Panzhihua ilmenite concentrate with coke, *Can. Metall. Q.*, 51(2012), No. 4, p. 434.

[8] G.Q. Zhang and O. Ostrovski, Reduction of ilmenite concentrates by methane-containing gas: Part I. Effects of ilmenite composition, temperature and gas composition, *Can. Metall. Q.*, 40(2001), No. 3, p. 317.

[9] G.Q. Zhang and O. Ostrovski, Reduction of ilmenite concentrates by methane-containing gas: Part II: Effects of preoxidation and sintering, *Can. Metall. Q.*, 40(2001), No. 4, p. 489.

[10] Y. Lei, Y. Li, J.H. Peng, W. Li, L.B. Zhang, and R.D. Wan, Carbothermic reduction of Panzhihua oxidized ilmenite in a

microwave field, *ISIJ Int.*, 51(2011), No. 3, p. 337.

[11] Z.F. Yuan, X.Q. Wang, C. Xu, W.B. Li, and M. Kwauk, A new process for comprehensive utilization of complex titania ore, *Miner. Eng.*, 19(2006), No. 9, p. 975.

[12] V.E. Roshchin, A.V. Asanov, and A.V. Roshchin, Possibilities of two-stage processing of titaniferous magnetite ore concentrates, *Russ. Metall.*, 2011(2011), No. 6, p. 499.

[13] Y.S. Sun, Y.X. Han, P. Gao, Z.H. Wang, and D.Z. Ren, Recovery of iron from high phosphorus oolitic iron ore using coal-based reduction followed by magnetic separation, *Int. J. Miner. Metall. Mater.*, 20(2013), No. 5, p. 411.

[14] G. Wang, Y.G. Ding, J.S. Wang, X.F. She, and Q.G. Xue, Effect of carbon species on the reduction and melting behavior of boron-bearing iron concentrate/carbon composite pellets, *Int. J. Miner. Metall. Mater.*, 20(2013), No. 6, p. 522.

[15] S.Y. Chen, P.H. Guo, X.L. Wu, and M.S. Chu, New process of metallization reduction–magnetic concentration–electroheat melting separation for vanadium titano-magnetite, *J. Northeast. Univ. Nat. Sci.*, 34(2013), No. 3, p. 378.

[16] M.S. Chu, M.X. Ai, F.M. Shen, and J.I. Yagi, Mathematical modeling of blast furnace operation with charging carbon composite briquette based on multi-fluid model, *Res. Iron Steel*, 35(2007), No. 1, p. 12.

[17] M.S. Chu, Z.G. Liu, Z.C. Wang, and J.I. Yagi, Fundamental study on carbon composite iron ore hot briquette used as blast furnace burden, *Steel Res. Int.*, 82(2011), No. 5, p. 521.

[18] M.S. Chu, J.I. Yagi, and H. Nogami, Numerical evaluation on lower temperature operation of blast furnaces by charging carbon composite agglomerates, *Steel Res. Int.*, 78(2007), No. 1, p. 10.